

Autodetachment spectroscopy and dynamics of CH_2CN^- and CD_2CN^-

K. R. Lykke, D. M. Neumark,^{a)} T. Andersen,^{b)} V. J. Trapa, and W. C. Lineberger
*Joint Institute for Laboratory Astrophysics, University of Colorado and National Bureau of Standards,
and Department of Chemistry and Biochemistry, University of Colorado, Boulder, Colorado 80309-0440*

(Received 20 July 1987; accepted 28 August 1987)

The technique of autodetachment spectroscopy is utilized in a study of two electronic states of CH_2CN^- and CD_2CN^- . The ground electronic state is a normal valence state while the outermost electron in the excited state is bound by the dipole moment of the neutral radical. Autodetachment occurs from excited rotational levels of this dipole bound state, giving some 5000 sharp features near the photodetachment threshold. All of these features were assigned and spectroscopic constants for both states are reported. The binding energy of the electron in this latter state is determined to be $\lesssim 66 \text{ cm}^{-1}$ and analysis of the autodetachment spectrum shows the electron affinities of CH_2CN and CD_2CN to be $\sim 12\,500$ and $\sim 12\,430 \text{ cm}^{-1}$, respectively. The dynamics of the autodetachment process is studied and various mechanisms for detachment are described.

I. INTRODUCTION

Before 1983, C_2^- and OH^- were the only negative ions studied by high-resolution spectroscopy.¹⁻⁴ Within the last few years, there has been a flurry of interest in the spectroscopy and structure of negative ions. There are two reasons for this delay compared with positive ion studies. First, it is difficult⁵ to produce an anion concentration sufficiently high to carry out absorption spectroscopy and yet have sufficiently simple absorbing samples to be interpretable. Second, the outer electron in negative ions is usually bound by less than $\sim 3 \text{ eV}$, so that there is very little "room" in which to have another bound state to carry out electronic spectroscopy from the ground state. Negative-ion spectroscopy has lagged behind neutral and positive-ion spectroscopy mainly because of these two issues.

The conventional spectroscopic method is measurement of the absorption of a beam of light by the absorbing species. Since negative ions occur in only low concentration, it was essential to increase the sensitivity of absorption spectroscopy in order to observe negative ions in the gas phase. A major improvement in absorption spectroscopy of negative ions (and positive ions) has been the introduction of velocity modulated spectroscopy.⁶ The negative ions that have been observed by this technique are typically the most abundant negative ions in the plasma⁷⁻⁹ (OH^- , FHF^- , NH_2^-) and are down in concentration from positive ions by only ~ 2 - 3 orders of magnitude. A very desirable feature of direct absorption spectroscopy is its complete generality. Some drawbacks to this technique include limited ion mass selectivity and large Doppler widths (most ions observed by direct absorption have been seen in hot plasma environments which are required to obtain high ion concentrations).

One method for circumventing the small concentration problem is to form a beam of negative ions and detect each

photon adsorbed with high efficiency via the method of *product* detection. This can be done if each negative ion that absorbs a photon is excited to a state above the detachment continuum, and subsequently decays by autodetachment ("autodetachment spectroscopy"). Each electron and neutral formed by this process can be detected with near unity efficiency. Mass selectivity is an additional feature of this method; by adding a momentum or energy selector to the ion beam, one can be sure of the mass of the ion that is detected. Also, by using a coaxial ion beam-laser beam geometry,⁹ one is able to obtain greatly reduced Doppler widths. A drawback of autodetachment spectroscopy is that the upper state of the transition has to lie above the detachment threshold; no bound states can be probed by this technique.

The upper level in autodetachment spectroscopy can be a vibrationally excited level of the same electronic state as the lower level, or it can belong to an excited electronic state. The first case, vibrational autodetachment spectroscopy, has been used¹⁰ to obtain the vibration-rotation spectrum of NH^- . When applicable, this is a very good method for determining the structural characteristics of the ion and for obtaining detailed information on the interaction between the rotating and vibrating neutral and the detached electron. The crucial drawback to this technique is that it is not general. The electron affinity of the neutral must be less than the vibrational interval in the negative ion in order for this approach to be successful.

Electronic autodetachment spectroscopy can be used to study ions with much higher electron affinities. An excited electronic state near the detachment threshold is required. While valence excited states of negative ions are uncommon, the recent observation of dipole bound electronically excited states of anions greatly expands the scope of ions accessible by autodetachment spectroscopy. These electronically excited states are the negative ion counterparts of Rydberg states in neutral molecules. A neutral molecule has an infinite number of Rydberg states, bound by the $1/r$ potential between the positive ion core and the electron, and converging to the ionization limit of the neutral molecule. Since

^{a)} Permanent address: Department of Chemistry, University of California, Berkeley, California 94720.

^{b)} 1984-85 JILA Visiting Fellow. Permanent address: Institute of Physics, University of Aarhus, Denmark.

there is no $1/r$ long-range potential between the neutral core and the electron in an anion, there are no Rydberg states in negative ions. However, a molecule with dipole moment greater than ~ 2 D will bind an electron in the $1/r^2$ potential and produce a Rydberg-type dipole bound state (DBS).^{12–17} These states are weakly bound (typically $\lesssim 100$ cm^{-1}) relative to the neutral molecule, the electron in a very diffuse orbital, and the DBS is structurally similar to the neutral core, much like a Rydberg state. However, there are only one or two of these dipole bound electronic states for each dipolar neutral molecule, unlike the infinity of Rydberg states in each neutral molecule.

We can exploit these facts about dipole bound states and use them to our advantage in negative ion spectroscopy. Transitions from the ground electronic state of the negative ion to the DBS will yield autodetachment resonances in the upper, unbound rotational–vibrational levels. This will give structural information about the anion ground state and the DBS, and hence the neutral core. Also, since the electron is bound by the anisotropic $1/r^2$ dipole potential, the study of the autodetaching resonances will give information about the interaction between a rotating–vibrating dipole and an electron. This will build understanding of the process of autoionization in neutral molecules, where only a few systems have been studied with rotational resolution.

Previous studies of dipole bound states have left gaps in our understanding of their properties. The best system for study would appear to be a diatomic anion. However, FeO^- was quite complicated¹⁸ because it has considerable electronic angular momentum associated with the core, producing very complex resonant structure that obscured the simple dipole bound states. The strongly polar NaCl^- ion was studied briefly,¹⁹ but no resonances were observed in the threshold photodetachment region. It is likely that the very large dipole of NaCl (~ 10 D) produced dipole bound states that were bound too tightly for rapid autodetachment. Consequently, the excited vibrational–rotational levels of the DBS lived too long to be observable in our apparatus. Lacking a suitable diatomic system, the next best system would be a simple^{16,17,20–24} polyatomic. Acetaldehyde enolate^{16,17} (CH_2CHO^-) was a good starting point for DBS studies because of the small binding energy (~ 5 cm^{-1}). However, the paucity of resonances (~ 20) obscured the autodetachment dynamics. Acetyl fluoride enolate²⁴ (CH_2CFO^-) has numerous autodetaching features because of the larger binding energy (~ 30 cm^{-1}), but the asymmetry of the molecule complicates the dynamics. Therefore, CH_2CN^- seems like a very good choice for DBS studies. It looks very much like a linear dipole (CCN skeleton) with perturbing hydrogens.

We chose CH_2CN^- for this study in part because it is known to have an electron affinity^{20,21} within the frequency range of cw tunable single mode laser technology. Also, although the CH_2CN dipole moment is not known, it should be on the order of 3–5 D and should bind at least one electronic DBS.^{20,23}

We have reported^{17–19} the study of a few dipole bound systems including a preliminary report²² on CH_2CN^- . In this paper, we will briefly detail the experimental apparatus and explain the autodetachment spectra we observe in

CH_2CN^- and some of the structural details we can extract from the spectroscopy. Finally, we go into some detail on the autodetachment lifetimes and try to elucidate mechanisms that are operative in negative ions in general and CH_2CN^- in particular.

II. EXPERIMENTAL

The coaxial laser–ion beam apparatus has been described in detail previously, and will be only briefly outlined.^{3(b),17} The basic system consists of a mass selected negative ion beam interacting collinearly with the output of a tunable laser with the products of photodetachment collected and counted. An ~ 500 pA beam of CH_2CN^- is formed by extraction from a hot cathode discharge source²¹ containing CH_3CN and NH_3 (total pressure ~ 0.1 Torr), mass selection with a 90° sector magnet, and acceleration to 2650 eV. The ions are then bent 90° by a transverse quadrupolar electric field²⁵ and merged for ~ 30 cm with the output of a home-built tunable ring dye laser. The neutrals that are formed by detachment are separated from the ion beam by a second quadrupole deflecting electric field and strike a KDP or CaF_2 plate. The impact produces secondary electrons which are detected by an electron multiplier and counted to yield the total photodetachment cross section. The electrons that are detached in the interaction region are collected by a weak solenoidal field (~ 5 G) and counted with a second electron multiplier. This electron collector can be used (with a reduced **B** field) as a discriminator that collects only threshold electrons, but was used in the total detachment cross section mode for this experiment.

The data were taken by scanning the laser in frequency (measured with a λ meter²⁶) while monitoring the neutrals and electrons formed as a function of photon frequency and normalized to the ion current and laser power. Using styryl 9 dye, the laser operates from about 790 to 870 nm with outputs of ~ 400 mW broadband and ~ 150 mW single mode when pumped with ~ 5 W all lines from an Ar II laser. The dye laser is easily configured in either a standing wave, broadband mode (birefringent tuner only, $\Delta\nu \sim 1$ cm^{-1}) or in single mode ($\Delta\nu < 1$ MHz). The resolution of this spectrometer is better than 30 MHz, limited by the Doppler spread in the kinematically compressed ion beam.^{3(b)}

III. OBSERVED SPECTRA

Photoelectron spectroscopy of CH_2CN^- has shown²¹ EA(CH_2CN) to be 1.543 ± 0.014 eV, and threshold photodetachment studies yield²³ 1.560 ± 0.006 eV, so in any case transitions to dipole bound states from the ground electronic state of CH_2CN^- should occur at ~ 800 nm. Figure 1 shows a 800 cm^{-1} scan of photodetachment from CH_2CN^- and CD_2CN^- near the photodetachment threshold. The resolution of the apparatus as configured for these scans was ~ 1 cm^{-1} (~ 30 GHz), and the maximum count rate was ~ 50 000 counts/s.

There are two processes at work in this photon energy region. One is direct photodetachment from populated vibrational–rotational levels of the negative ion ground state to a number of (neutral + electron) continua.²⁷ This is a

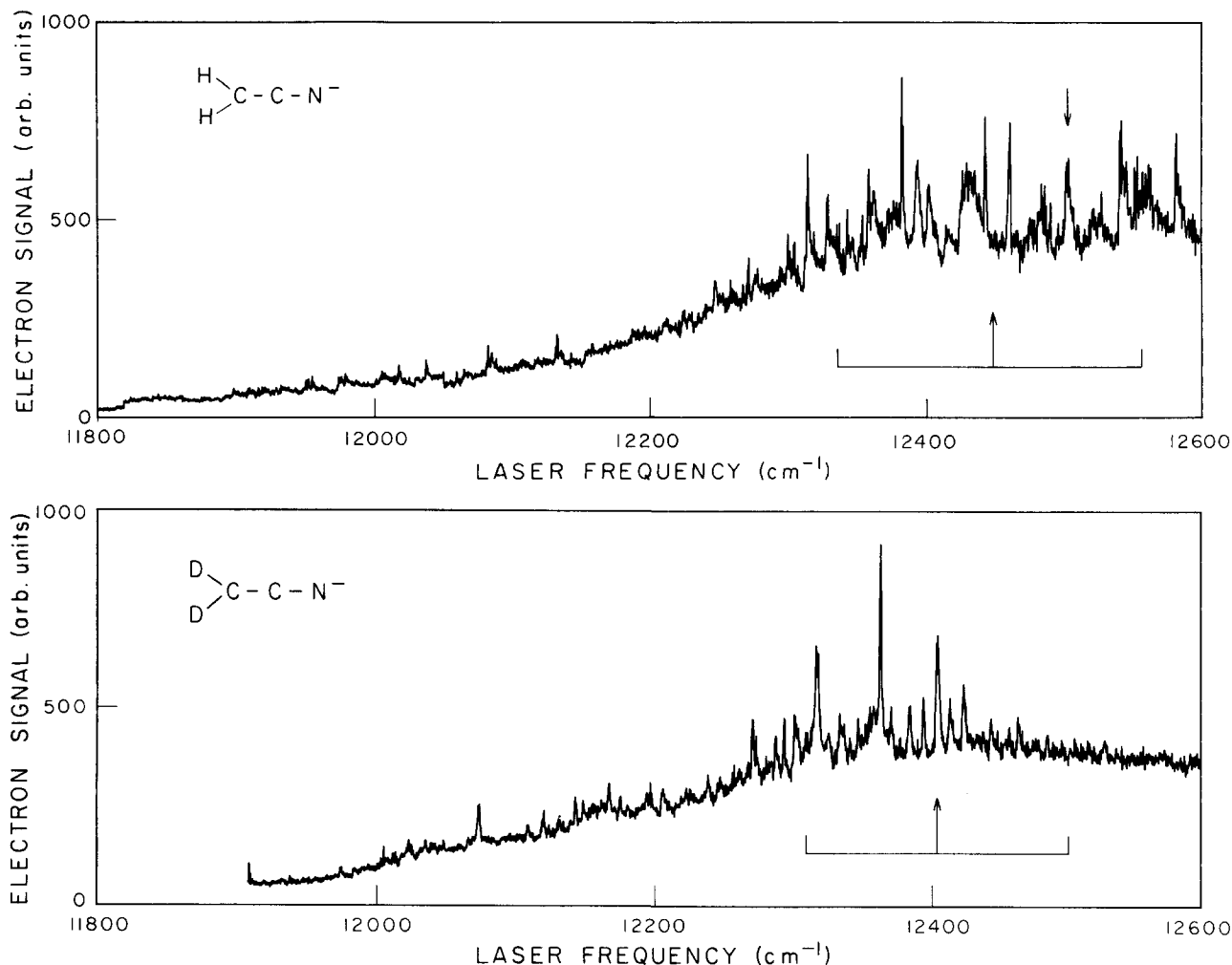


FIG. 1. Broadband scans of (a) CH_2CN^- and (b) CD_2CN^- . Resolution in these scans is $\sim 1 \text{ cm}^{-1}$ (30 GHz). The arrows located at the bottom of each figure signify the location of the electron affinity determined in Ref. 1. The arrow above the spectrum for CH_2CN^- shows the region "blown up" in Fig. 2.

"bound-free" process with a large number of unresolved vibrational-rotational thresholds, with typical cross sections $\sim 10^{-18} \text{ cm}^2$. These cross sections change slowly with energy, giving rise to the gentle slope in Fig. 1. The second process involved is a transition from the ground ion state to an excited dipole bound state of the anion which then autodetaches. This "bound-quasibound" process produces the sharp spikes in Fig. 1.

The spiked structure centered around $12\,430 \text{ cm}^{-1}$ [$12\,360 \text{ cm}^{-1}$ for CD_2CN^- , Fig. 1(b)] results from an unresolved (in this figure) group of transitions from the lowest vibrational state of the anion to the lowest vibrational state of the DBS. The structure centered at $12\,000 \text{ cm}^{-1}$ ($12\,090 \text{ cm}^{-1}$ for CD_2CN^-) is due to a hot band transition from a vibrational excited state of the anion to the lowest vibrational state of the DBS.

The specific type of electronic transition involved and details of the rotational fine structure are not obvious in Fig. 1, so the structured region was scanned at higher resolution to identify the rotational transitions involved. Marks *et al.*²³ have used a lower resolution ion cyclotron resonance photo-

detachment apparatus to assign the rotational branches, as discussed later.

Shown in Fig. 2 is an approximately 200-fold magnification of the marked feature in Fig. 1(a). The resolution here is $\sim 20 \text{ MHz}$, limited by the Doppler spread in the ion beam. Most of the spectral region shown in Fig. 1 was scanned with this resolution. Approximately 5000 lines were tabulated (with $\sim 0.01 \text{ cm}^{-1}$ precision) throughout the range from $11\,900$ to $12\,600 \text{ cm}^{-1}$ and the spectroscopic assignment will be discussed in the next section.

IV. SPECTROSCOPIC ANALYSIS

CH_2CN^- is a near prolate asymmetric top (see Fig. 3) having C_{2v} symmetry (see Sec. V) with the a axis along the C_2 axis. The bound-quasibound transitions seen in CH_2CN^- are \perp -type, with the transition moment along the c axis.²⁸ This \perp transition gives corresponding selection rules for the rotational quantum numbers: $\Delta K_a = \pm 1$, $\Delta J = 0, \pm 1$. The branches are labeled by a left superscript for ΔK_a , a capital letter for ΔJ , and K_a in the lower state as a

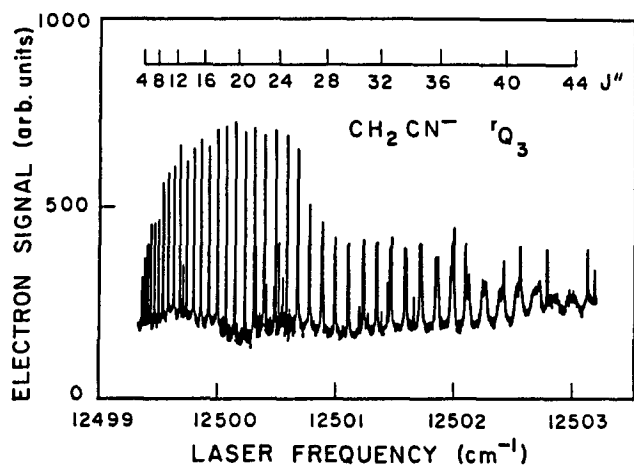


FIG. 2. High resolution (~ 20 MHz) scan of a typical Q branch in CH_2CN^- . The lower J 's lie toward the left of the figure. Notice the broadening of the lines toward high J . This figure is a "blow up" of the region indicated by an arrow above the spectrum in Fig. 1(a).

right subscript (e.g., the rQ_3 branch is shown in Fig. 2; this is the $\Delta K_a = +1, \Delta J = 0$ transition from $K'' = 3$ to $K' = 4$). An energy level diagram and some representative transitions are shown in Fig. 4.

The spectroscopic assignments were carried out in several steps. One can estimate the rotational constants for CH_2CN^- from typical bond lengths²¹ ($A \approx 10 \text{ cm}^{-1}$, $B \approx C \approx 0.3 \text{ cm}^{-1}$). Since $A \gg B, C$ the Q branch transitions tend to form clumps separated by $\sim 2 \text{ \AA}$ ($\sim 20 \text{ cm}^{-1}$ for CH_2CN^- and $\sim 10 \text{ cm}^{-1}$ for CD_2CN^-). Once the Q branches were found, the corresponding P and R branches could be assigned. The missing lines of a given K stack at low J give the correct K values for both lower and upper states, provided that they are missing only because $J \geq K$. However, at low K , some additional J 's were missing because they did not detach (see below), and not simply due to the fact that J can never be less than K . The lack of lower J 's was a hindrance in assigning the spectra, but once the analysis was complete for the higher J 's, the transition frequencies for the lower J 's could be predicted. From these predicted values, the lower J 's could then be identified and assigned.

Another hindrance in autodetachment spectroscopy is that the spectral lines become broad and the spectrum unassignable when the upper state lifetime gives broad reson-

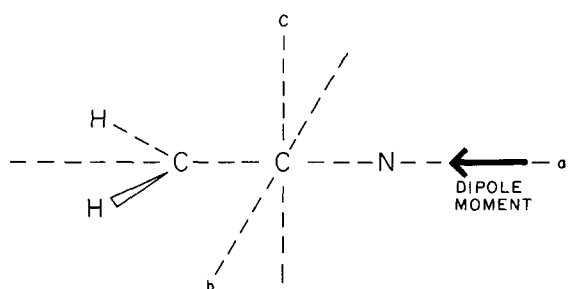


FIG. 3. Schematic diagram of the structure of the radical CH_2CN . The three inertial axes and the direction of the dipole moment are shown, with the hydrogens lying in the plane of the molecule. Approximate distances from Ref. 21 are $R(\text{CN}) \approx 1.16 \text{ \AA}$, $R(\text{CC}) \approx 1.39 \text{ \AA}$, and $R(\text{CH}) \approx 1.08 \text{ \AA}$.

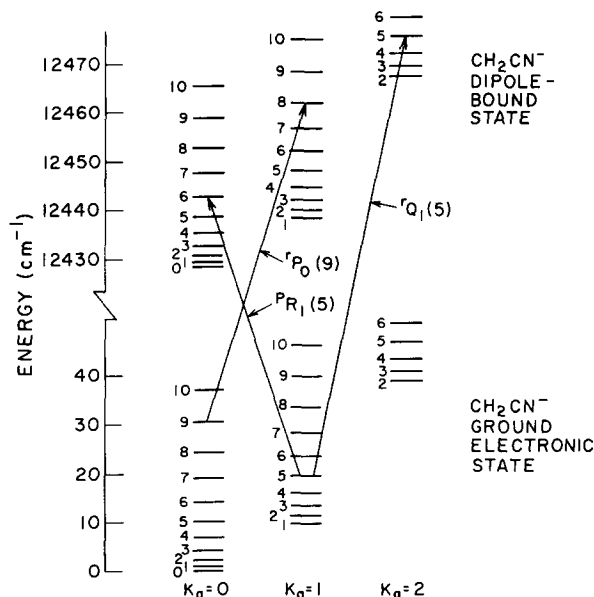


FIG. 4. Partial energy level diagram for CH_2CN^- . The asymmetry doubling is not shown. A few representative optical transitions are depicted with the appropriate labels.

ances. For the systems reported here, only the ground vibrational state of the DBS could be fully assigned. The spectrum for CH_2CN^- and CD_2CN^- was scanned from $\sim 11\,600$ to $\sim 13\,200 \text{ cm}^{-1}$ and only the regions between $11\,900$ and $12\,600 \text{ cm}^{-1}$ contained sharp structure. Broad clumps were observed in regions where transitions to higher vibrational levels of the DBS might be expected, but no assignments could be performed. As discussed later, this result shows that vibrational excited states of the DBS live less than ~ 300 ps.

The CH_2CN^- and CD_2CN^- spectra are quite different from that seen¹⁷ for acetaldehyde enolate, CH_2CHO^- . One difference is that CH_2CHO^- has C_s symmetry while CH_2CN^- has C_{2v} symmetry. This manifests itself in the spectra by labeling the two hydrogens as identical: the nuclear spin statistics²⁸ make transitions that start from odd K''_a a factor of 3 more intense than those that start from even K''_a . In CD_2CN^- , transitions that originate from even K''_a levels are a factor of 2 more intense than those that start from odd K''_a .

A more fundamental difference between CH_2CN^- and CH_2CHO^- is that the former has a larger dipole moment and will bind an electron more tightly. The principal consequence for the spectroscopic analysis is that there are many more long-lived states in the DBS in CH_2CN^- than in CH_2CHO^- . This allows us to fit the data to Watson's²⁹ reduction S Hamiltonian including quartic centrifugal distortion

$$\begin{aligned}
 H = & \left[A - \frac{B+C}{2} \right] J_z^2 + \left(\frac{B+C}{2} \right) J^2 \\
 & - D_J J^4 - D_{JK} J^2 J_z^2 - D_K J^4 \\
 & + \left[\frac{B-C}{4} + d_1 J^2 \right] (J_+^2 + J_-^2) \\
 & + d_2 (J_+^4 + J_-^4), \quad J_{\pm} = J_x \pm iJ_y. \quad (1)
 \end{aligned}$$

TABLE I. Spectroscopic constants for CH_2CN^- and CD_2CN^- .^a

	CH_2CN^- ground state		DBS	CD_2CN^- ground state		DBS
	$\nu = 0^+$	$\nu = 1^+$	$\nu = 0$	$\nu = 0^+$	$\nu = 1^+$	$\nu = 0$
A (cm^{-1})	9.294 31(14)	8.696 05(60)	9.510 35(17) 9.513 10(63)	4.695 17(15)	4.493 74(27)	4.771 27(11) 4.771 76(40)
B (cm^{-1})	0.338 427(20)	0.337 430(39)	0.341 049(21) 0.341 140(43)	0.300 372(11)	0.300 146(19)	0.302 318(11) 0.302 266(19)
C (cm^{-1})	0.327 061(21)	0.327 825(38)	0.328 764(21) 0.328 980(43)	0.283 102(11)	0.284 299(20)	0.283 821(11) 0.283 715(21)
D_J (cm^{-1})	$1.65(10) \times 10^{-7}$	$1.61(21) \times 10^{-7}$	$2.19(10) \times 10^{-7}$ $2.70(21) \times 10^{-7}$	$1.056(44) \times 10^{-7}$	$0.935(77) \times 10^{-7}$	$1.347(46) \times 10^{-7}$ $1.152(78) \times 10^{-7}$
D_{JK} (cm^{-1})	$1.297(15) \times 10^{-5}$	$2.033(51) \times 10^{-5}$	$1.499(14) \times 10^{-5}$ $1.544(45) \times 10^{-5}$	$0.773 9(78) \times 10^{-5}$	$0.790(13) \times 10^{-6}$	$0.961 0(65) \times 10^{-5}$ $0.972(22) \times 10^{-5}$
D_K (cm^{-1})	$1.002 8(21) \times 10^{-3}$	$-0.146(30) \times 10^{-3}$	$0.754 6(36) \times 10^{-3}$ $0.757 0(270) \times 10^{-3}$	$0.237 1(44) \times 10^{-3}$	$0.117 9(76) \times 10^{-3}$	$0.185 5(20) \times 10^{-3}$ $0.211 9(135) \times 10^{-3}$
d_1 (cm^{-1})	$-0.90(18) \times 10^{-8}$	$-9.18(38) \times 10^{-8}$	$1.65(27) \times 10^{-8}$ $2.19(80) \times 10^{-8}$	$-0.10(16) \times 10^{-8}$	$-0.129(87) \times 10^{-8}$	$-0.79(15) \times 10^{-8}$ $-0.38(12) \times 10^{-8}$
d_2 (cm^{-1})	$-0.586(77) \times 10^{-8}$	$0.97(17) \times 10^{-8}$	$0.191(70) \times 10^{-8}$ $-0.59(13) \times 10^{-8}$	$-0.270(41) \times 10^{-8}$	$-0.129(87) \times 10^{-8}$	$-0.378(40) \times 10^{-8}$ $-0.38(12) \times 10^{-8}$
T (cm^{-1})	0	424.770(5) [12 003.895(4)]	12 428.665(2)	0	289.129(4) [12 071.305(3)]	12 360.434(1)
Δ_{ad} (in $\text{amu } \text{Å}^2$)	-0.082 7	-0.474 6	0.074 4 0.054 5	-0.166 5	-0.620 4	0.100 8 0.113 8
σ (cm^{-1})		0.013 5	0.013 8		0.009 1	0.005 9

^a Note: The constants were fit with a least-squares routine using Watson's reduction S Hamiltonian. Included in the table are the results from four different fits representing the four different bands observed in the study. The numbers in parentheses represent 1σ . The two different entries for the DBS represent the results of the fit for the 0-0 band (upper entry) and the hot band (lower entry). The number of transitions included in the fits were 1298 (0-0 band of CH_2CN^-), 618 (hot band of CH_2CN^-), 841 (0-0 band of CD_2CN^-), and 741 (hot band of CD_2CN^-). The quantity σ corresponds to the standard deviation of the fit to the entire band.

The results of each of the four fits are shown in Table I. The complete line list with assignments is contained in Ref. 30.

As mentioned earlier, we also observe transitions from an excited vibrational state of the negative ion to the ground vibrational level of the DBS. There are two methods for determining the excited state, and thus the lower state. The linewidths of the transitions label the DBS's quantum numbers; these were identical in both the 0-0 transition centered at $\sim 12 430 \text{ cm}^{-1}$ for CH_2CN^- ($12 360 \text{ cm}^{-1}$ for CD_2CN^-) and the hot band transition centered at $\sim 12 000 \text{ cm}^{-1}$ ($12 090 \text{ cm}^{-1}$ for CD_2CN^-). Also, the DBS spectroscopic constants were similar but not identical for both vibrational bands (see Table I). Presumably, a perturbation observed in the excited vibrational state caused some small problems in the fit (see below). The nuclear spin statistics for this excited vibrational state in the ground electronic state label it as the ($\nu = 1^+$) umbrella mode in CH_2CN^- . As explained by Moran *et al.*²¹ (see also Ref. 31), the actual assignment of the active vibrational mode requires careful consideration of all vibrational modes in the molecule. Since the vibrational frequency shifts to a large extent upon deuteration (424.77 cm^{-1} for CH_2CN^- compared to 289.13 cm^{-1} for CD_2CN^-) the vibrational motion must include hydrogens. Only five out of the nine vibrational modes in CH_2CN contain substantial hydrogenic motion. The asymmetric and symmetric C-H stretches will be $\sim 3000 \text{ cm}^{-1}$

and much too high in frequency to account for the observed vibration. Also, the CH_2 scissors and CH_2 rock motions should be $\sim 1000 \text{ cm}^{-1}$ (as explained in Ref. 31). Therefore, the observed vibrational hot band corresponds to a transition from the second excited vibrational state ($\nu = 1^+$) of the umbrella motion. The $\nu = 0^+ \rightarrow \nu = 1^+$ spacings are shown in Table I.

There was only one observed perturbation in all of the spectra. This occurred in the vibrationally excited state (umbrella mode) of the ground electronic state of CH_2CN^- . It shows up in $K = 0$ with an approximately quadratic dependence on J (i.e., the observed levels are shifted by $\sim 0.2 \text{ cm}^{-1}$ at $J \approx 30$ and go up to $\sim 0.3 \text{ cm}^{-1}$ by $J \approx 40$). A problem in assigning the perturbation is that the lowest J observed is 23 (see later). The standard deviation of the spectroscopic fit without the $K' = 1 \leftarrow K'' = 0$ transitions is 0.012 cm^{-1} and increases to 0.036 cm^{-1} when these transitions are included. The constants shown in Table I are obtained without including the $K' = 1 \leftarrow K'' = 0$ transitions.

The perturbation is very isolated, and there is little information to be obtained from it. However, since there is an approximate quadratic dependence on J , it would appear to be a Coriolis-induced perturbation.²⁸ The only vibrations in CH_2CN^- that are low enough in frequency to cause this perturbation are the two C-C-N bends (in-plane and out-of-plane). Since the perturbed (observed) vibration is of A_1

symmetry, either the in-plane (B_2) or out-of-plane (B_1) vibration can be causing the perturbation. At this time we have no plausible explanation for the negative D_k constant in the $v = 1^+$ state other than the fact that the perturbation has different influences on different K_a stacks.

V. STRUCTURE

These data provide a limited amount of structural information on CH₂CN⁻, as is always the case in high resolution spectroscopy of polyatomic molecules with a limited number of isotopic substitutions. However, our results provide insight on the planarity of the ground and dipole bound states of the anion. The presence of the 3:1 intensity alternation (odd K_a'' :even K_a'') for CH₂CN⁻ (2:1 for even K_a'' :odd K_a'' in CD₂CN⁻) implies that the vibrational states transform according to a point group including the operator C_2^a . This means that CH₂CN⁻ either has a planar equilibrium configuration or is in different vibrational levels associated with inversion of the CH₂CN⁻ but having a pyramidal equilibrium configuration. The intensity alternations thus rule out a *rigid* pyramidal CH₂CN⁻ skeleton, and imply that the molecule is at least sampling the planar part of the potential some of the time. This is the same situation seen in NH₂CN³² (isoelectronic with CH₂CN⁻).

One of the methods for determining planarity of molecules is by examination of the inertial defect.³³ The inertial defect is defined by

$$\Delta_{\text{id}} = I_c - I_a - I_b, \quad (2)$$

where I_x = moment of inertia about the x axis. Usually, if Δ_{id} is zero or a small positive number, the molecule can be considered planar, but if Δ_{id} is negative the molecule can be considered³³ nonplanar. However, zero point vibrational motion can change the situation. Out-of-plane vibrational modes tend to make the inertial defect more negative, while in plane vibrational modes tend to make Δ_{id} more positive. Included in Table I are the inertial defects for the six vibrational states (three for CH₂CN⁻, three for CD₂CN⁻) we have observed.

The inertial defects for the two dipole bound states are both small and positive. This confirms that the DBS is planar. Since the DBS should look like the radical (analogous to Rydberg states resembling the positive core), we have experimental evidence for the planarity of the CH₂CN radical.

The negative inertial defects for the ground electronic states for both isotopes show that we are dealing with some out-of-plane vibration. In the preceding section, we concluded that the hot band seen in CH₂CN⁻ arises from a transition from an excited umbrella vibration in the ground electronic state to the ground vibrational state of the DBS. Since the excited vibrational state has a much more negative inertial defect than the zero point vibrational states and the deuterio isotope has an even larger (negative) Δ_{id} , one could be tempted to say that CH₂CN⁻ is nonplanar. However, we already know that CH₂CN⁻ exhibits C_{2v} symmetry (identical H's) in all observed vibrational levels, so that the molecule is at least "sampling" some planar structure. In large, floppy molecules known to be planar,³⁴ negative inertial de-

fects have been identified with the large amplitude out-of-plane motions. However, in such cases when the inertial defects are plotted against vibrational quantum number in the out-of-plane vibration, a straight line is obtained.³⁴ The inertial defect obtained by extrapolation to $v = -1/2$ at the vibrationless state is then found³⁴ to be positive, in accord with the known planarity of the molecule. This same situation would appear to hold here. If the two Δ_{id} 's for each isotopic species are extrapolated to $v = -1/2$, a small positive inertial defect (0.7–0.11 amu Å²) is obtained. However, we are not able to say anything about a small barrier to inversion seen by Moran *et al.*²¹ The CH₂CN⁻ photoelectron spectroscopy experiment performed by Moran *et al.* yields data that are more sensitive to the out-of-plane angle of the CH₂ than are the present experiments. The reason for this is that their photoelectron spectroscopy experiment accesses many more vibrational states of the neutral than our experiment does, so their potential energy function is more sensitive.

While the difficulties described above preclude a quantitative determination of structural parameters for the ground state of the anion, the planarity of the dipole-bound state permits us to extract some information concerning bond lengths and bond angles for the DBS. There are four parameters to be determined (R_{CH} , R_{CC} , R_{CN} , and $\angle\text{HCH}$) assuming a planar C_{2v} molecule. There are also in principle four pieces of information available from the six rotational constants determined for the *h*-DBS and *d*-DBS. It is not possible to obtain a precise r_0 structure from these data, but a number of structural inferences may be drawn. First, the ratio $A_{\text{H}}/A_{\text{D}}$ should be $m_{\text{D}}/m_{\text{H}}$ for a rigid molecule. The observed ratio differs from the deuterium/hydrogen mass ratio by about 5%, indicating the presence of substantial hydrogen motion with respect to the CCN axis. Another indication of significant hydrogen motion is that, if all bond lengths are held constant, then we find that the optimum HCH bond angle is some 3° larger than the corresponding DCD bond angle. With this caveat in mind, a brief description of the fitting procedure is presented.

The parameters A , B , and C for both isotopic species were fit to rotational constants obtained for a rigid planar molecule, with bond lengths and angles which did not change upon isotopic substitution. The quantities best determined in such a fit are $R_{\text{CH}} \sin(\angle\text{HCH}/2)$ and $(R_{\text{CN}} + R_{\text{CC}})$. A fit was first attempted for CD₂CN since the lower amplitude hydrogenic motions should make structure determination less problematic. The fairly large inertial defect of course prevents a perfect fit between the experimental data and the model. The results of this fitting procedure are given below:

$$\left. \begin{aligned} \angle\text{HCH} &= (118 \mp 200 D \pm 3)^\circ \\ R_{\text{CH}} &= (1.07 \pm D \pm 0.02) \text{ \AA} \end{aligned} \right\} |D| < 0.05$$

and

$$\left. \begin{aligned} R_{\text{CN}} &= (1.165 \mp \Delta \pm 0.02) \text{ \AA} \\ R_{\text{CC}} &= (1.395 \pm \Delta \pm 0.02) \text{ \AA} \end{aligned} \right\} |\Delta| < 0.1 \text{ \AA}$$

The quantities D and Δ show the degree of correlation between parameters. The range of D or Δ is that which re-

sults in a doubling of the residuals of the fit to all of the rotational constants. The final number in the error is that change in bond length or angle which is required to double the residuals of a fit to the rotational constants. The correlation between parameters is clearly apparent. When these same parameters were employed to fit the CH_2CN data, all parameters were essentially at a local minimum except $\angle\text{HCH}$. Increasing this angle from 118° to 122.4° gave an essentially perfect fit between the model and the experimental data.

VI. AUTODETACHMENT LIFETIMES AND BINDING ENERGY OF THE DBS

Figure 5(a) depicts a single mode scan over a Q branch transition to $K' = 2$, showing several interesting phenomena in CH_2CN^- . The most obvious point is that the lowest J 's are missing. This is even more evident in Fig. 5(b), which shows transitions to $K' = 1$. Another interesting feature in Fig. 5(a) is the increasing width of the lines as J increases. Both of these phenomena can be understood in terms of a model of the autodetachment mechanisms and energetics.

As mentioned in the Introduction, a transition is observed only if the upper level of the transition autodetaches while the excited anion is located in the interaction region.

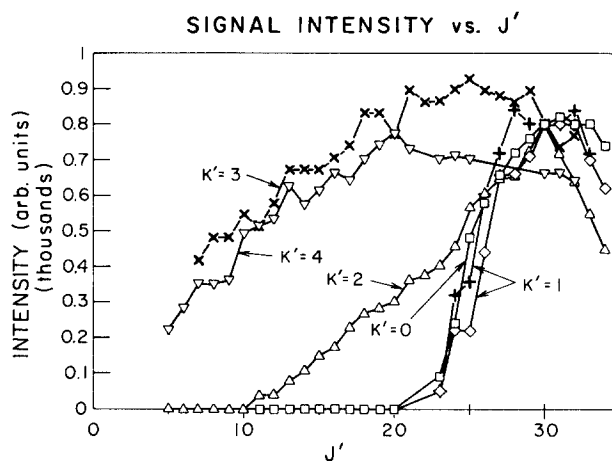


FIG. 6. A graph of relative intensities in several branches in CH_2CN^- . The peak intensities were obtained from continuous scans on a chart recorder, not from the computer-spliced data shown in Figs. 2 and 5.

The length of time spent in the interaction region is

$$\frac{d}{v} = \frac{25 \text{ cm}}{1 \times 10^7 \text{ cm/s}} \approx 2.5 \mu\text{s}. \quad (3)$$

Therefore, if the autodetachment lifetime is more than a few microseconds longer than this, the molecules that are excited will either fluoresce or hit the Faraday cup as negative ions and in either case will not be counted as autodetachment signal. This will tend to make the observed signal vary directly with the autodetachment rate. Shown in Fig. 6 is a graph of intensity vs rotational quantum number for a few different branches. Two branches ($K' = 3, 4$) are sufficiently far above the onset of the detachment continuum that their width is not limited by the 20 MHz Doppler instrument resolution, and three ($K' = 0, 1, 2$) have apparent widths which are limited solely by the Doppler width (i.e., $\Delta\nu \lesssim 20 \text{ MHz}$). The branches with $K' = 3$ and 4 have a width determined by lifetime broadening:

$$\Delta\nu \geq \frac{1}{2\pi\Delta\tau}, \quad (4)$$

and these branches show a normal intensity distribution (at least to $J = 30$), characteristic of a thermal distribution of initial states and a perpendicular transition of a near-prolate rotor. However, the branches with $K' = 0, 1, 2$ that have Doppler-limited linewidths at low J show an intensity increasing linearly with J . This observation allows us to extrapolate to obtain the linewidths of the longest lived levels. For example, for $K' = 2$, this procedure yields autodetachment width that increases from $\approx 1 \text{ MHz}$ at $J = 11$ to $\approx 20 \text{ MHz}$ at $J = 30$, which is approximately the Doppler-limited linewidth.

If the autodetachment rate and fluorescence rate are about the same order of magnitude, we also have the possibility of decreasing intensity. If a molecule is pumped up to a certain J, K level (say, an Q branch, shown in Fig. 7) there are several alternative pathways to deexcite the anion. We measure the autodetachment channel only. Therefore, if the sum of the optical transition rates out of the excited state are

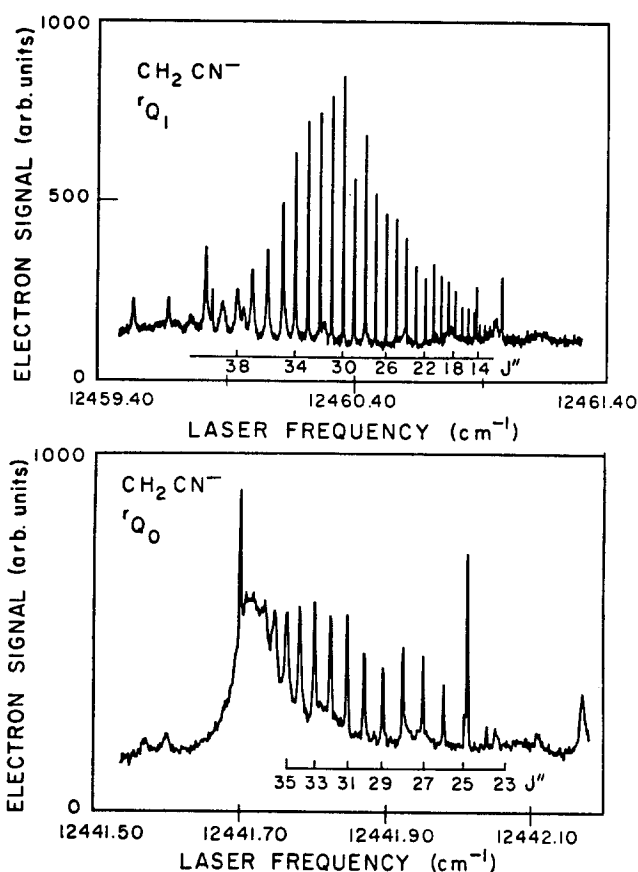


FIG. 5. Two Q branches showing the lack of observation of lower J 's in $K' = 2$ (a) and $K' = 1$ (b). The lower J 's missing in this figure were also not observed in the P and R branches.

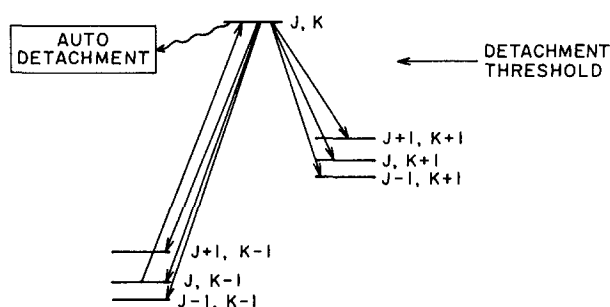


FIG. 7. Schematic diagram showing one optical (laser-induced) transition to an excited state and several pathways out of this excited state. The upward (downward) straight arrows signify absorption (emission) of photons, whereas the wavy arrow shows electron detachment.

much greater than the autodetachment rate, the intensity will be abnormally low.

The resonance linewidths were obtained by scanning the laser while measuring both the detachment signal and Fabry-Perot fringes spaced by ~ 250 MHz (see Fig. 8). A few of the lines were carefully fit to Lorentzians, a procedure which gave approximately the same result as measuring the full width at half-maximum by hand (within 20%), so the remaining lines were cataloged using the latter method. Shown in Figs. 9(a) and 9(b) are the experimentally determined linewidths (FWHM) vs total rotational quantum number J for some selected K_a stacks in CH_2CN^- and CD_2CN^- . The two notable features are the relatively small change in detachment rate with increasing J up to $J \cong 32$ and the rapid rise in detachment rate after this point. This rapid rise occurs in the same range of J for all of the K stacks in CH_2CN^- . Figure 10 displays the linewidths for both isotopes as a function of both J and K to present this point in a more detailed view. We now try to explain all of the observed autodetachment features in CH_2CN^- .

Figure 11 is a simplified energy level diagram for both the CH_2CN^- DBS and the CH_2CN radical, using the DBS rotational constants for both species. Much like Rydberg states, we expect the structures of these two states to be very similar. This expectation has been borne out in the DBS of acetaldehyde enolate¹⁷ (CH_2CHO^-) and vinoxy radical³⁵ (CH_2CHO) where the rotational constants are within 1% of each other. Since microwave data are not available for the CH_2CN radical, this procedure gives us the best levels avail-

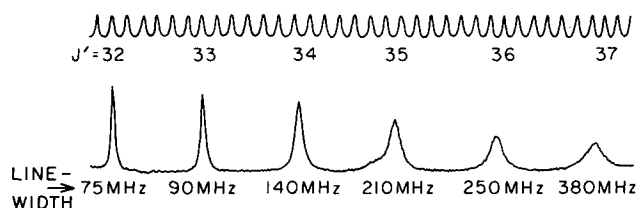


FIG. 8. Chart recording of typical data showing the rapid increase of the linewidth at high J . The data were obtained by sending the output of the electron multiplier into a discriminator and then into a rate meter and then into the y input of a chart recorder. The markers at the top of the figure are Fabry-Perot fringes (250 MHz spacing) recorded simultaneously.

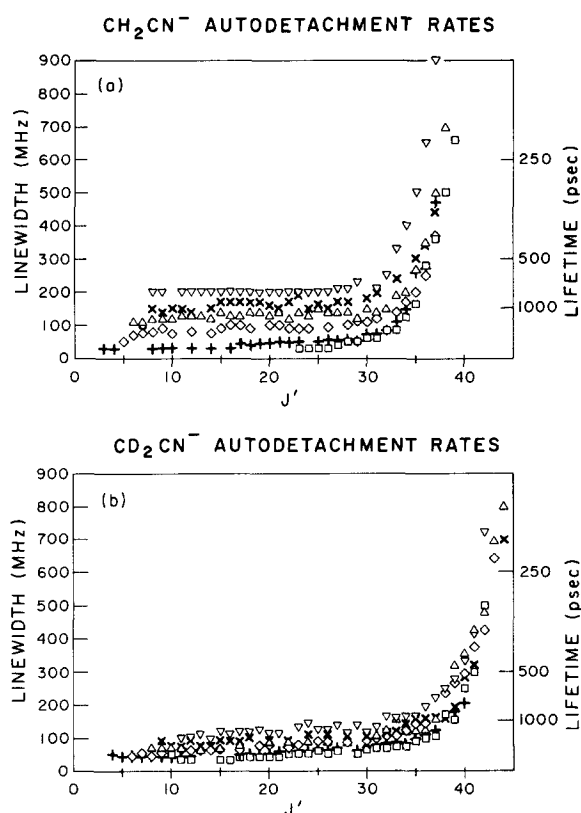


FIG. 9. Experimentally measured linewidths as a function of rotational quantum number for a few K' stacks. (a) CH_2CN^- : $\square, K' = 1$; $+, K' = 3$; $\diamond, K' = 5$; $\triangle, K' = 6$; $\times, K' = 7$; $\nabla, K' = 8$. (b) CD_2CN^- : $\square, K' = 3$; $+, K' = 4$; $\diamond, K' = 6$; $\triangle, K' = 8$; $\times, K' = 9$; $\nabla, K' = 11$.

able at present. Also shown schematically is the continuum for the electron and neutral and some typical autodetachment transitions. The continuum onset is indicated to occur just below the lowest observed autodetaching level ($J = 9, K_a = 2$) in the CH_2CN^- DBS. This observation places a rigorous upper limit on the binding energy of the DBS of ~ 67 cm^{-1} , and, from the term value for the DBS, gives an electron affinity of $\sim 12\,500$ cm^{-1} . However, the binding energy could be even lower than this if the nonobserved lower states live too long to be seen in our apparatus.

Marks *et al.*²³ obtained a binding energy of ~ 160 cm^{-1} , based upon lower resolution data (comparable to Fig. 1) where individual rotational levels were not resolved and a model that assumes no variation in lifetimes of the upper states. The resolved spectra reported here show this assumption to be inaccurate, leading to too high a binding energy for CH_2CN^- . A related assumption was used in the assignment²³ of the CD_2CN^- spectra, and in this case the more closely spaced levels lead to an incorrect numbering of the CD_2CN^- K stacks (i.e., the branch labeled $K' = 3 \leftarrow K'' = 2$ in their Table I should be labeled $K' = 1 \leftarrow K'' = 0$, and so on for the other branches).

There are several important selection rules governing autodetachment from CH_2CN^- . A rigorous selection rule is that a J, K level must decay via $\Delta K_a = 0, \pm 2, \pm 4, \dots$ due to the identical H's around the C_{2v} (a) axis (no nuclear spin exchange). A propensity rule is that the transition should

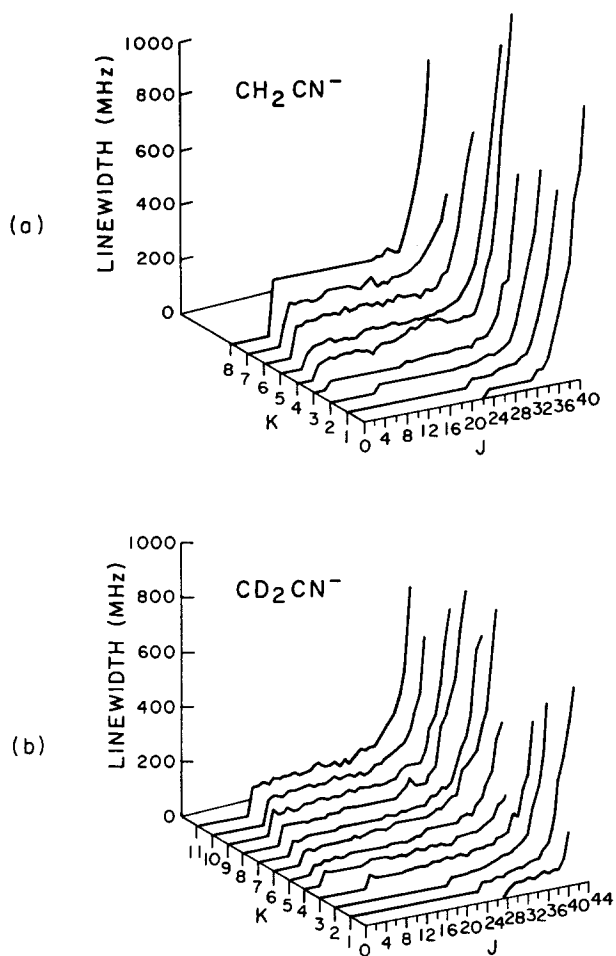


FIG. 10. Three-dimensional projection of the linewidth variation as a function of J and K : (a) CH_2CN^- , (b) CD_2CN^- .

take place with the minimum possible change in angular momentum. Shown in Fig. 11 by curved arrows are some representative autodetaching transitions. Only even K stacks and only a few J levels are shown for clarity. Transitions labeled *A* correspond to $\Delta J = -5$ or -4 and $\Delta K = 0$. These are the only electron detachment pathways open to the lowest observed levels in $K = 0$ and $K = 1$. All DBS $K = 0, 1$ levels below this autodetach so slowly that either we cannot observe them in our apparatus or the levels are bound, e.g., $J \lesssim 13$ in $K = 0$. The slow decay rate of those levels for which autodetachment is energetically possible is due to the large change in J which would be required for autodetachment. The transition *B* corresponds to $\Delta J \cong -5$ and $\Delta K = -2$, the smallest ΔJ channel open for the low J 's in $K = 2$. The two different types of channels open for $K = 0, 1$ and $K = 2$ manifest themselves in the different slopes shown in Fig. 6 for the different observed intensities. Transition *C* ($\Delta K = -2, \Delta J = -2$) represents a process energetically allowed for the higher K stacks, a small ΔJ accompanied by a $\Delta K = -2$. The transitions labeled *D* illustrate the reason for the rapid increase in the autodetachment rate beginning $J \approx 33$ (≈ 38 for CD_2CN^-). This process corresponds to a $\Delta J = -3$ and $\Delta K = 0$ transition and first becomes energetically allowed at the same value of J, J_T , regardless of K . The

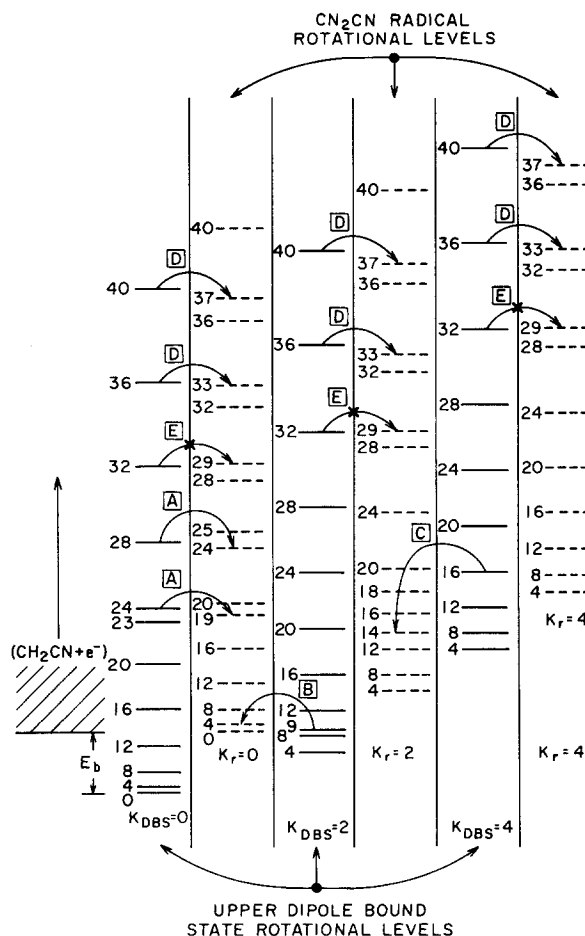


FIG. 11. Simplified energy level diagram showing several different pathways for detachment. The diagram has been drawn assuming a binding energy of $\sim 60 \text{ cm}^{-1}$ for the DBS. Only a few J levels in the even K stacks are shown for clarity. The letters labeling a few of the autodetaching transitions signify *A*, the transitions observed from the low J levels in $K = 0, 1$ (i.e., $\Delta J \geq 4, \Delta K = 0$); *B*, the transitions observed from the low J levels in $K = 2, 3$ (i.e., $\Delta J \geq 4, \Delta K = -2$); *C*, the transitions observed from the low J levels in the high K stacks (i.e., $\Delta J = \Delta K = -2$); *D*, the transitions observed from the high J levels in all of the K stacks (i.e., $\Delta J \leq 3, \Delta K = 0$); and *E*, the transitions that are not observed due to energy conservation. The fast turn on in rate at $J \approx 33$ for CH_2CN^- (≈ 38 for CD_2CN^-) occurs due to process *D* taking over.

region of an abrupt rise in autodetachment corresponds to a binding energy of $E_b \lesssim 6BJ_T$ where B is the effective rotational constant for end-over-end rotation ($\sim 0.33 \text{ cm}^{-1}$ for CH_2CN^-) and J_T is the "turn-on" value. The reason for the value, $6BJ_T$, for the energy difference is that rotational levels are separated in energy by $\Delta E = 2BJ\Delta J$. Above $J \approx 40$, the transitions into the continuum are so rapid that the higher J 's are not distinguishable.

Since the lowest observed level in the CH_2CN^- DBS has $\sim 67 \text{ cm}^{-1}$ rotational energy, the binding energy must be smaller than this. An intriguing possibility is that the rapid turn on in autodetachment rate at $J \approx 33$ corresponds to an $E_b \lesssim 4BJ$ (44 cm^{-1}) and that the rapid rate change is due to the opening of the $\Delta J = -2$ channel. In fact, the lowest level observed in CD_2CN^- is ($J' = 9, K' = 3$) and also implies a binding energy of $\lesssim 66 \text{ cm}^{-1}$ for the CD_2CN^- DBS. In fact, $K' = 3$ can only detach to $K' = 1$, which leads to an

estimate of 62 cm⁻¹. In light of these facts, we cannot totally determine which exact channel opening ($\Delta J = 2$ or $\Delta J = 3$) is responsible for the rapid increase in rate.³⁶ However, we can state with certainty that autodetachment is inhibited for $\Delta K \neq 0$ transitions. In the following section, we will explore some of the reasons for these selection rules in rotational autodetachment of CH₂CN⁻.

VII. AUTODETACHMENT MECHANISMS

The phenomenon of autodetachment (autoionization) arises from the breakdown of the Born–Oppenheimer approximation, namely, due to terms that in the molecular Hamiltonian couple the bound state to the continuum. From these couplings, we can calculate transition rates into the continuum via the Golden Rule³⁷

$$\begin{aligned} \text{rate} &\propto \frac{2\pi}{\hbar} |\langle \psi_f | \mathbf{T} | \psi_i \rangle|^2 \rho \\ &\propto \frac{2\pi}{\hbar} k^{2l+1} |\langle \psi_f | \mathbf{T}' | \psi_i \rangle|^2, \end{aligned} \quad (5)$$

where \mathbf{T} is the coupling operator, ψ_i is the negative ion (DBS) wave function, ψ_f is the electron plus neutral wave function, and ρ is the density of states; in the second form, k and l are the linear and angular momenta of the leaving electron, and \mathbf{T}' is the energy independent coupling operator. There are *four* different types of coupling operators of significance in molecular autodetachment.³⁷ These are as follows: (1) configuration interaction (electron–electron), (2) spin–orbit, (3) vibrational–electronic, and (4) rotational–electronic. We will briefly discuss each of these and show that the only coupling mechanism operative in the lowest vibrational level of the DBS is rotation–electronic coupling.

Configuration interaction driven autoionization has been studied in a few systems³⁸ for autoionization and arises from electron–electron repulsion. This coupling will only induce autodetachment if the neutral *electronic* state lies below the negative ion *electronic* state. From Fig. 11, we see this is not the case, so this mechanism of coupling to the continuum is not operative here. Spin–orbit autoionization (autodetachment) has recently been studied in several systems³⁹ and occurs when a molecular core can make a spin–orbit change to a lower state to allow the electron to leave the molecule. However, asymmetric top molecules cannot have electronic orbital angular momentum²⁸ (i.e., no axial symmetry to which to couple the electron) so that this type of coupling is inactive in CH₂CN⁻.

Both vibration–electronic and rotation–electronic coupling are driven by the nuclear kinetic energy operator \mathbf{T}_R ,

$$\mathbf{T}_R = \mathbf{T}_{\text{vib}} + \mathbf{T}_{\text{rot}} \cong -\frac{\hbar^2}{2M} \frac{d^2}{dR^2} - \frac{\hbar^2}{2MR^2} \mathbf{N}^2, \quad (6)$$

acting on the electronic wave function. There has been a great deal of theoretical^{37,40–42} and experimental⁴³ effort devoted to vibration–electronic coupling. Since the autodetaching transitions studied in this paper originate from the ground vibrational state of the DBS, the vibration–electronic terms will be unimportant. However, in the spectral range covered, we do observe sequence bands to higher (unknown) vibrational states. These sequence bands were com-

posed of broad lines (> 500 MHz) which were too weak and too broad to obtain a rotational analysis. Presumably these vibrationally excited states of the DBS decay by vibration–electronic coupling, and at a rate generally more rapid than for those analyzed levels reported here.

The remaining form of autodetachment arises from rotation–to–electronic coupling. This process has not been studied as much as vibration–electronic coupling because: (1) most autoionization studies have not had rotational resolution; (2) when other mechanisms are available, rotation–electronic coupling will usually be negligible in comparison; (3) in autoionization, the longest range force is the Coulomb force which dwarfs the dipolar force in most molecules.

The form of the coupling operator is given by the following expression³⁷:

$$\mathbf{T}_{\text{rot}} \propto -\frac{\hbar^2}{2m_e R^2} \mathbf{N}_{\text{el}} \cdot \mathbf{N}_{\text{rot}}. \quad (7)$$

This operator is similar in form to Λ -type doubling; as the molecule rotates faster and faster, the electron becomes uncoupled from the axis. In neutral Rydberg diatomic molecules, there is a transition from Hund’s case (a) [or case (b)] to Hund’s case (d) as n (the principal hydrogenic quantum number of the Rydberg molecule) increases. This is due to the fact that the orbital angular momentum of the outer electron “sees” an isotropic Coulomb core⁴⁴ as the electron’s orbital radius increases. This physical effect is very similar to rotational autodetachment from dipole bound states, where the anisotropic dipole binding force begins to be averaged out.

In order to understand the rotational autodetachment process, we need first to understand the rotational motion of CH₂CN⁻. The classical motion of a prolate symmetric top ($A \gg B \approx C$) is described in Refs. 45 and 46. As stated in Sec. IV, J is the total angular momentum of the molecule and K_a is the component of the angular momentum along the a inertial axis for a prolate top. The angular momentum vector \mathbf{J} is fixed in space while the figure axis nutates about it at frequency $2BJc$ and the molecule rotates about the figure axis at frequency $2(A - B)Kc$. Since $A \gg B$, what this means in relation to CH₂CN⁻ is that J motion tends to rotate the C–C–N in an end-over-end fashion; whereas K motion tends to rotate the H’s around the a axis (Fig. 12). This means that high J ’s will rotate the dipole moment, regardless of K , whereas $J \approx K$ does not rotate the dipole moment. Since the DBS electron must remain near the positive end of the dipole to be bound, rotation that moves the dipole axis is destabilizing. Therefore, the higher J ’s should decouple the electron

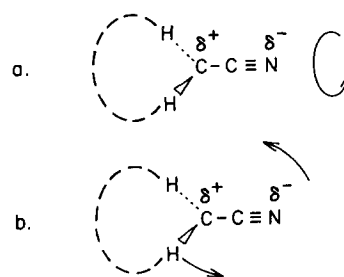


FIG. 12. Schematic of CH₂CN⁻ showing two different types of limiting behavior in the rotational motion: (a) corresponds to $J \approx K$, (b) corresponds to $J \gg K$. The dotted line shows the qualitative shape of the DBS orbital, but it should be expanded a factor of ~ 30 to show the correct size of the orbital.

more rapidly than the higher K 's, even though the higher K 's are much higher in energy. For example, $J = 40$, $K = 0$ lies $\sim 350 \text{ cm}^{-1}$ lower than $J = 30$, $K = 8$ but the former auto-detaches at least three times more rapidly. This effect is perhaps better seen in a classical picture, as follows.

Suppose that the only force binding the electron in the DBS were the dipolar force, given by a *point* dipole potential $U(r, \theta)$. The radial dipole force $F_{\text{dip}}(r, \theta)$ would then be

$$F_{\text{dip}} = -\frac{\partial U}{\partial r} = -\frac{\partial(eD \cos \theta / 4\pi\epsilon_0 r^2)}{\partial r} = \frac{2eD \cos \theta}{4\pi\epsilon_0 r^3}, \quad (8)$$

where e is the electron charge, in Coulombs; D is the dipole moment, in Debyes ($3.3 \times 10^{-30} \text{ C m D}^{-1}$); r is the electron distance from the dipole; and θ is the angle between the dipolar axis and the electron's position.

Now, the force that will decouple the electron from the dipole will be the centrifugal force, given by

$$F_{\text{cent}}(r) = \frac{m_e v^2}{r} = \frac{m_e (2\pi r \nu_{\text{rot}})^2}{r} = 4\pi^2 m_e r \nu_{\text{rot}}^2, \quad (9)$$

where m_e is the mass of the electron, r is the electron's distance from the dipole, and ν_{rot} is the rotational frequency of the dipole given by

$$\nu_{\text{rot}} = 2 B c \sqrt{J(J+1)} \approx 2 B c J, \quad (10)$$

where B = rotational constant (in cm^{-1}) of dipole, c = speed of light, J = rotational quantum number of the dipole.

If Eq. (10) is substituted into Eq. (9) and the forces $F_{\text{dip}}(r, \theta)$ and $F_{\text{cent}}(r)$ are set equal, the resulting relation between r and J corresponds to complete decoupling of the electron from the rotational axis

$$r_{\text{dip}}^4 = \left(\frac{2eD}{4\pi\epsilon_0} \right) \left(\frac{1}{16\pi^2 m_e B^2 c^2 J(J+1)} \right). \quad (11)$$

That is, the electron will not be able to follow the dipole and will lag behind. This lag in turn produces a catastrophic ejection because the $\cos \theta$ dependence of the dipole force weakens the restoring force as the electron "slips behind." We know that since the abrupt turn on occurs at $\sim J = 33$ for CH_2CN^- , the distance r_{dip} from the dipole of the electron that is bound to the dipole is given by

$$r_{\text{dip}} = 68 \text{ \AA}.$$

We can obtain the radius of the electron orbit in another way by using our binding energy of $\sim 60 \text{ cm}^{-1}$ and assuming a dipole moment of 3.5 D. The relation

$$E_{\text{bind}} = -\frac{eD}{4\pi\epsilon_0 r_{\text{dip}}^2} \quad (12)$$

then gives $r_{\text{dip}} \cong 36 \text{ \AA}$. Of course, we do not know either the exact binding energy of the DBS or the exact dipole moment for CH_2CN , but the fact that these two values for the radius of the electron orbit are within a factor of 2 is satisfying. While this classical view is self-consistent, it cannot be taken literally, since the electron de Broglie wavelength is comparable with r_{dip} . An 80 cm^{-1} electron has a 120 \AA de Broglie wavelength.

One part of autodetachment (autoionization) that has not been discussed in detail is the role the angular momentum barrier,

$$E_{\text{barrier}} \propto \frac{\hbar^2 l(l+1)}{2mr^2}, \quad (13)$$

plays in determining the autodetachment rate. This has not been dealt with in autoionization because the Coulomb force overwhelms this force for the different partial waves. This is why the cross section for photoionization has a constant value, independent of l (the angular momentum of the leaving electron), at threshold in contrast to the threshold behavior for photodetachment which is given by⁴⁷

$$\sigma \propto k^{2l+1}. \quad (14)$$

The combination of the angular momentum barrier and the anisotropic dipole binding makes an extremely complicated trajectory for the leaving electron. The electron is bound to the electropositive end of CH_2CN until it becomes decoupled. The electron does not "feel" the angular momentum barrier until it starts to decouple from the internuclear axis and assumes a value of l , the orbital angular momentum of the leaving electron. Therefore, we have a problem that could be dealt with by a frame transformation⁴⁸; i.e., a totally body centered frame at the start, transforming to a lab fixed frame at the end. This full procedure has not yet been attempted for CH_2CN^- autodetachment, but Clary⁴⁹ has taken a substantial step in this direction. He calculates rotationally adiabatic CH_2CN^- DBS potentials, in which the autodetaching levels appear as Feshbach resonances. Initial agreement is encouraging, and inclusion of $\Delta J > 1$ transitions promises quantitative understanding of this process.

VIII. NONOBSERVATION OF ELECTRIC FIELD STRIPPING

The quadrupole deflector which terminates the coaxial interaction region provides a transverse electric field which can be used qualitatively to study electric field stripping of specific rotational levels of the dipole bound state. If an optically excited level of the DBS, bound or unbound, lives longer than a few μs , then the excited ion will proceed from the coaxial interaction into the quadrupole deflector. If the electric field of the quadrupole deflector produces field ionization, then a signal will be seen on the neutral detector, but not on the slow electron detector. This method was used¹⁷ to observe the bound levels in acetaldehyde enolate's dipole bound state (AEDBS). We expected to see similar electric field stripping in CH_2CN^- , but extensive searches at wavelengths where these bound states were known to exist gave *no* hint of electric field induced stripping. Levels bound by $\sim 5 \text{ cm}^{-1}$ in AEDBS were field stripped by only $\sim 70 \text{ V/cm}$; whereas similarly bound states in CH_2CN^- were not affected by 5 kV/cm . We now try to account for such behavior.

Inspection of the appropriate energy level diagrams shows that the bound levels in AEDBS could be stripped with a change in angular momentum of $\Delta J \lesssim 2$, but the levels with similar binding energy in CH_2CN^- require at least $\Delta J \gtrsim 14$ (see Fig. 11). However, these levels could strip with a low ΔJ if the stripping process removed $\sim 50 \text{ cm}^{-1}$ instead

of just 5 cm^{-1} . A much larger electric field would be required in this case. We are not set up at present to vary the electric field in a quantitative fashion, but this would clearly be an interesting experiment.

IX. CONCLUSIONS

Autodetachment spectroscopy of CH_2CN^- has yielded much information on many of the properties of dipole bound states. Any molecule with a dipole moment $\gtrsim 2 \text{ D}$ will bind an electron in a weakly bound, large orbital, much like Rydberg states. The study of these states with rotational resolution has given considerable insight into the dynamics of the detachment process. It should now be possible to predict which negative ions can be studied with autodetachment spectroscopy.

ACKNOWLEDGMENTS

We would like to thank K. K. Murray and D. G. Leopold for obtaining a photoelectron spectrum of room temperature CH_2CN^- . We would also like to thank S. Moran and G. B. Ellison for stimulating discussions about CH_2CN^- . This research was supported by NSF Grant Nos. CHE 83-16628 and PHY 86-04504. The spectroscopic analyses were carried out on the JILA VAX 8600.

- ¹G. Herzberg and A. Lagerqvist, *Can. J. Phys.* **46**, 2363 (1968).
- ²W. C. Lineberger and T. A. Patterson, *Chem. Phys. Lett.* **13**, 40 (1972).
- ³(a) P. L. Jones, R. D. Mead, B. E. Kohler, S. D. Rosner, and W. C. Lineberger, *J. Chem. Phys.* **73**, 4419 (1980); (b) U. Hefter, R. D. Mead, P. A. Schulz, and W. C. Lineberger, *Phys. Rev. A* **28**, 1429 (1983); (c) R. D. Mead, U. Hefter, P. A. Schulz, and W. C. Lineberger, *J. Chem. Phys.* **82**, 1723 (1985).
- ⁴H. Hotop, T. A. Patterson, and W. C. Lineberger, *J. Chem. Phys.* **60**, 1806 (1974); P. A. Schulz, R. D. Mead, P. L. Jones, and W. C. Lineberger, *ibid.* **77**, 1153 (1982).
- ⁵H. Massey, *Negative Ions* (Cambridge University, Cambridge, 1976).
- ⁶R. J. Saykally, *Spectroscopy* **1**, 40 (1986).
- ⁷N. H. Rosenbaum, J. C. Owrtusky, L. M. Tack, and R. J. Saykally, *J. Chem. Phys.* **84**, 5308 (1986); B. D. Rehffuss, M. W. Crofton, and T. Oka, *ibid.* **85**, 1785 (1986); L. M. Tack, N. H. Rosenbaum, J. C. Owrtusky, and R. J. Saykally, *ibid.* **84**, 7056 (1986).
- ⁸K. Kawaguchi and E. Hirota, *J. Chem. Phys.* **84**, 2953 (1986).
- ⁹B. A. Huber, T. M. Miller, P. C. Cosby, H. D. Zeman, R. L. Leon, J. T. Moseley, and J. R. Peterson, *Rev. Sci. Instrum.* **48**, 1306 (1977); S. M. Trujillo, R. H. Neynaber, and E. W. Rothe, *ibid.* **37**, 1655 (1966); W. H. Wing, G. A. Ruff, W. E. Lamb, and J. J. Spezeski, *Phys. Rev. Lett.* **36**, 1488 (1976).
- ¹⁰D. M. Neumark, K. R. Lykke, T. Andersen, and W. C. Lineberger, *J. Chem. Phys.* **83**, 4364 (1985).
- ¹¹O. H. Crawford, *Proc. Phys. Soc. (London)* **91**, 279 (1967).
- ¹²W. R. Garrett, *Chem. Phys. Lett.* **5**, 393 (1970).
- ¹³W. R. Garrett, *Phys. Rev. A* **3**, 961 (1971).
- ¹⁴J. E. Turner, *Am. J. Phys.* **45**, 758 (1977).
- ¹⁵W. R. Garrett, *J. Chem. Phys.* **73**, 5721 (1980); **77**, 3666 (1982).
- ¹⁶A. H. Zimmerman and J. I. Brauman, *J. Chem. Phys.* **66**, 5823 (1977); R. L. Jackson, A. H. Zimmerman, and J. I. Brauman, *ibid.* **71**, 2088 (1979); R. L. Jackson, P. C. Hiberty, and J. I. Brauman, *ibid.* **74**, 3705 (1981).
- ¹⁷R. D. Mead, K. R. Lykke, W. C. Lineberger, J. Marks, and J. I. Brauman, *J. Chem. Phys.* **81**, 4883 (1984); K. R. Lykke, R. D. Mead, and W. C. Lineberger, *Phys. Rev. Lett.* **52**, 2221 (1984).
- ¹⁸T. Anderson, K. R. Lykke, D. M. Neumark, and W. C. Lineberger, in *Electronic and Atomic Collisions*, edited by D. C. Lorents, W. E. Meyerhof, and J. R. Peterson (Elsevier, Amsterdam, 1986), pp. 791–798; T. Andersen, K. R. Lykke, D. M. Neumark, and W. C. Lineberger, *J. Chem. Phys.* **86**, 858 (1987).
- ¹⁹K. R. Lykke, D. M. Neumark, and W. C. Lineberger (unpublished results).
- ²⁰A. H. Zimmerman and J. I. Brauman, *J. Am. Chem. Soc.* **99**, 3565 (1977).
- ²¹S. Moran, H. B. Ellis, Jr., D. J. DeFrees, and G. B. Ellison, *J. Am. Chem. Soc.* **109**, 5996 (1987).
- ²²A preliminary report of this work is in K. R. Lykke, D. M. Neumark, T. Andersen, V. J. Trapa, and W. C. Lineberger, in *Laser Spectroscopy VII*, edited by Y. R. Shen and T. W. Hänsch (Springer, Berlin, 1985), pp. 130–133.
- ²³J. Marks, D. M. Wetzel, P. B. Comita, and J. I. Brauman, *J. Chem. Phys.* **84**, 284 (1986).
- ²⁴J. Marks, J. I. Brauman, R. D. Mead, K. R. Lykke, and W. C. Lineberger (to be submitted).
- ²⁵H. D. Zeman, *Rev. Sci. Instrum.* **48**, 1079 (1977).
- ²⁶S. A. Lee and J. L. Hall, *Appl. Phys. Lett.* **25**, 367 (1976).
- ²⁷K. J. Reed, A. H. Zimmerman, H. C. Andersen, and J. I. Brauman, *J. Chem. Phys.* **64**, 1368 (1976); A. R. P. Rau, *Comments At. Mol. Phys.* **14**, 285 (1984).
- ²⁸G. Herzberg, *Electronic Spectra of Polyatomic Molecules* (Van Nostrand, New York, 1967).
- ²⁹J. K. G. Watson, *J. Chem. Phys.* **46**, 1935 (1967); in *Vibrational Spectra and Structure*, edited by J. R. Durig (Marcel Dekker, New York, 1977), Vol. 16, pp. 1–89.
- ³⁰K. R. Lykke, Ph.D. thesis, University of Colorado, 1987.
- ³¹H. B. Ellis, Ph.D. thesis, University of Colorado, 1983.
- ³²D. J. Millen, G. Topping, and D. R. Lide, Jr., *J. Mol. Spectrosc.* **8**, 153 (1962).
- ³³T. Oka and Y. Morino, *J. Mol. Spectrosc.* **6**, 472 (1961); W. Gordy and R. L. Cook, *Microwave Molecular Spectra, Techniques of Chemistry* (Wiley, New York, 1984), Vol. 18.
- ³⁴R. K. Kakar, *J. Chem. Phys.* **56**, 1189 (1972).
- ³⁵Y. Endo, S. Saito, and E. Hirota, *J. Chem. Phys.* **83**, 2026 (1985).
- ³⁶One problem with finding the exact channel that opens is the uncertainty in the turn-on position. If the turn on occurs at $J' \cong 33$ for CH_2CN^- , then $E_b \leq 66.3 \text{ cm}^{-1}$ (for $\Delta J = -3$) or $E_b \leq 44.2 \text{ cm}^{-1}$ (for $\Delta J = -2$). If the turn on occurs at $J' \cong 38$ for CD_2CN^- , then $E_b \leq 66.8 \text{ cm}^{-1}$ (for $\Delta J = -3$) or $E_b \leq 44.5 \text{ cm}^{-1}$ (for $\Delta J = -2$). However, the turn-on position could actually be different for these two molecules.
- ³⁷R. S. Berry, *J. Chem. Phys.* **45**, 1228 (1966).
- ³⁸U. Fano, *Phys. Rev.* **124**, 1866 (1961).
- ³⁹H. Lefebvre-Brion, A. Giusti-Suzor, and G. Raseev, *J. Chem. Phys.* **83**, 1557 (1985); H. Lefebvre-Brion, P. M. Dehmer, and W. A. Chupka, *ibid.* **85**, 45 (1986).
- ⁴⁰J. N. Bardsley, *Chem. Phys. Lett.* **1**, 229 (1967).
- ⁴¹R. S. Berry and S. E. Nielsen, *Phys. Rev. A* **1**, 395 (1970).
- ⁴²J. Simons, *J. Am. Chem. Soc.* **103**, 3971 (1981); P. K. Acharya, R. A. Kendall, and J. Simons, *ibid.* **106**, 3402 (1984).
- ⁴³P. M. Dehmer and W. A. Chupka, *J. Chem. Phys.* **65**, 2243 (1976).
- ⁴⁴G. Herzberg and Ch. Jungen, *J. Mol. Spectrosc.* **41**, 425 (1972).
- ⁴⁵G. Herzberg, *Infrared and Raman Spectroscopy* (Van Nostrand, New York, 1945).
- ⁴⁶R. N. Zare, *Angular Momentum in Quantum Mechanics* (in press).
- ⁴⁷E. P. Wigner, *Phys. Rev.* **73**, 1002 (1948); A. R. P. Rau, *Comments At. Mol. Phys.* **14**, 285 (1984).
- ⁴⁸A. R. P. Rau and U. Fano, *Phys. Rev. A* **4**, 1751 (1971).
- ⁴⁹D. C. Clary, *J. Phys. Chem.* (submitted).